Acta Oceanol. Sin., 2021, Vol. 40, No. 10, P. 106–117
https://doi.org/10.1007/s13131-021-1848-5
http://www.aosocean.com
E-mail: ocean2@hyxb.org.cn

Evolution of the North Atlantic Current and Barents Ice Sheet as revealed by grain size populations in the northern Norwegian Sea during the last 60 ka

Weiguo Wang[1], Mengwei Zhao[2]*, Yanguang Liu[3], Min Jiang[1], Chengqiang Wu[1], Yang Liu[4]

[1] Third Institute of Oceanography, Ministry of Natural Resources, Xiamen 361005, China

[2] Pilot National Laboratory for Marine Science and Technology (Qingdao), Qingdao 266237, China

[3] First Institute of Oceanography, Ministry of Natural Resources, Qingdao 266061, China

[4] School of Earth Sciences, Lanzhou University, Lanzhou 730000, China

Received 10 April 2020; accepted 2 June 2021

Abstract

The grain size distribution of bulk sediment samples was decomposed in a core to reconstruct paleoceanographic evolution over the past 60 ka in the northern Norwegian Sea. The results show that sediments consisted of 3–4 grain populations derived from the North Atlantic Current (NAC) and Barents Ice Sheet (BIS). The grain size data suggest three palaeoceanographic evolution stages: (1) an environment affected by BIS and NAC and changed with the interstadial/stadial transition in phase with the Greenland ice-core record at 60–31 ka BP, during which discharge of icebergs and the content of the coarsest population containing ice-rafted debris (IRD) in the sediments increased significantly during stadial, while the fine silt population containing volcanic glasses increased with the enhancement of NAC during the interstadial; (2) an extreme environment controlled by BIS at 31–13 ka BP. BIS reached to its maximum at about 31 ka BP and the turbid plumes that formed at the leading edge of BIS contributed to a significant increase in the clayey population in sediments. Icebergs drained into the northern Norwegian Sea with periodical calving of the BIS at 31–19 ka BP. Subsequently, the ablation of the BIS discharged massive floods with clayey sediments and icebergs into the Norwegian Sea at 19–13 ka BP, resulting in a constant increase in clay and IRD in sediments; and (3) a marine environment similar to the present one under the strong influence of NAC following the complete melting of the BIS after 13 ka BP, NAC is the dominant transport agent and no IRD occurred in sediments. The fine silt populations containing volcanic glasses transported by NAC significantly increased.

Key words: Norwegian Sea, sediments, grain size population, North Atlantic Current, Barents Ice Sheet, paleoceanography, last glacial

Citation: Wang Weiguo, Zhao Mengwei, Liu Yanguang, Jiang Min, Wu Chengqiang, Liu Yang. 2021. Evolution of the North Atlantic Current and Barents Ice Sheet as revealed by grain size populations in the northern Norwegian Sea during the last 60 ka. Acta Oceanologica Sinica, 40(10): 106–117, doi: 10.1007/s13131-021-1848-5

1 Introduction

The Norwegian Sea is located on the pathway of the North Atlantic Current (NAC) to the Arctic Ocean (Latarius and Quadfasel, 2016). Part of the warm NAC sinks in the Norwegian Sea to initiate the Atlantic Meridional Overturning Circulation (AMOC), and the rest continues to flow northward to the Arctic Ocean (Hansen and Østerhus, 2000; Latarius and Quadfasel, 2016). During the last glaciation, the Barents Ice Sheet (BIS) extended to the Barents Shelf margin, massive amounts of icebergs and melt water discharged into the northern Norwegian Sea (Pope et al., 2016). Thus the melt water affected the amount of warm NAC entering the Norwegian Sea and its position in the water column (Ezat et al., 2014; Rasmussen et al., 2016), which led to changes in the AMOC, heat release from the NAC, and subsequently resulted in changes in ice cover in the Arctic Ocean and terrestrial climate (Broecker, 1991; Wang et al., 2020a). Thus, the Norwegian Sea is highly sensitive to global climate change (Dokken et al., 2013; Muschitiello et al., 2019). Research on the paleoceanographic evolution of the Norwegian Sea will provide deeper insights into the mechanisms of global climate change.

To date, many studies have been published on sediment cores collected from the northern slope of the Iceland-Shetland Ridge in the southern Norwegian Sea and from the Vøring Plateau in the eastern Norwegian Sea, with those sediment cores recording the changes in sea ice, seawater temperature, NAC inflow, water layer structure, and ocean ventilation (Bauch et al., 2001; Elliot et al., 2001; Meland et al., 2008; Rasmussen and Thomsen, 2008, 2009; Dokken et al., 2013; Simstich et al., 2013; Ezat et al., 2014, 2017; Sadatzki et al., 2019). However, few studies have been conducted on the Lofoten Basin in the northern Nor-

Foundation item: The Basic Scientific Research Operation Fee of the Third Institute of Oceanography, the Ministry of Natural Resources under contract No. 2018006; the project of the Chinese Arctic and Antarctic Administration of the State Oceanic Administration under contract No. CHINARE2016-03-02; the Shandong Provincial Natural Science Foundation under contract No. ZR2019BD054.

*Corresponding author, E-mail: yinwei_zhao@163.com

wegian Sea, which is an ideal place for studying the interaction between NAC and BIS. In addition, the existing paleoceanographic studies from the northern Norwegian Sea mainly used sediment cores collected at the base and slope of the Barents Shelf, which is an ideal site for studying BIS evolution, but not for the NAC record because the glacial sediments from the BIS suppress other information. In addition, these published records span ages shorter than 30 ka (Telesiński et al., 2015; Knies et al., 2018; Struve et al., 2019), and therefore fail to fully record the interaction between BIS and NAC in the northern Norwegian Sea during the last glaciation.

Granularity is the basis of sedimentology research and can provide information on the transportation and depositional environments of sediments. Most grain size distributions (GSDs) of hydraulic sediments are bimodal or polymodal, which are composed of various unimodal populations, and each population follows a certain distribution pattern and represents a different sediment source, transport and deposition process (Middleton, 1976; Ashley, 1978). By decomposing the GSDs into a number of unimodal populations and performing independent genesis analysis on each population combined with spatial and temporal comparisons among populations, it is possible to obtain more information than that from grain size parameters of bulk samples, which have been widely used in the research of loess, lakes, and marine sediments (Sun et al., 2002; Nagashima et al., 2012; Xiao et al., 2012; Park et al., 2014; Wang et al., 2020b).

Ice-rafted debris (IRD) is ubiquitous in high-latitude marine sediments (Ruddiman, 1977; Dowdeswell et al., 1999; Phillips and Grantz, 2001; Darby, 2003; Lisitzin, 2010), and is usually used as a proxy for ice sheet evolution. However, little attention has been paid to fine grains in sediments, which may provide important information about paleoceanography. Given this context, this study mathematically decomposes GSDs into a number of populations to decipher the evolution of NAC and BIS (fine and coarse grains in sediments respectively), and their interaction with the marine environment in the northern Norwegian Sea.

2 Regional background

The Nordic seas are located between Svalbard, Greenland, Iceland, and Scandinavia and connect the Arctic Ocean and the North Atlantic Ocean, bordering the North Atlantic Ocean at the Iceland-Shetland Islands in the south and the Arctic Ocean at the Fram Strait in the north (Fig. 1). The submarine ridges divide the Nordic seas into the Greenland Sea, Norwegian Sea, and Iceland Sea. The Norwegian Sea is located on the western side of Scandinavia, and its northeastern region is connected to the Barents Sea. At present, the surface circulation of the Nordic seas is primarily controlled by the warm NAC and cold East Greenland Current (EGC). The NAC flows into the Norwegian Sea with two branches, and one branch flows through the submarine ridge (500 m in depth) between the Iceland and Faroe Islands, and the other branch flows through a channel at a depth of more than 1 500 m between the Faroe and Shetland Islands (Wary et al., 2016). The NAC flows northward in the Norwegian Sea and finally enters the Arctic Ocean with two branches, one branch enters the Arctic Ocean through the Barents Sea, and the other branch enters the Arctic Ocean through the Fram Strait (Aksenov et al., 2010). The EGC flows into the Nordic seas from the west of the Fram Strait and flows southward along the edge of the Greenland Sea shelf, and finally flows out of the Denmark Strait (Hansen and Østerhus, 2000). The AMOC occurs while the northward-flowing NAC releases heat to the atmosphere, becomes denser, sinks and outflows over the Iceland-Shetland Ridge.

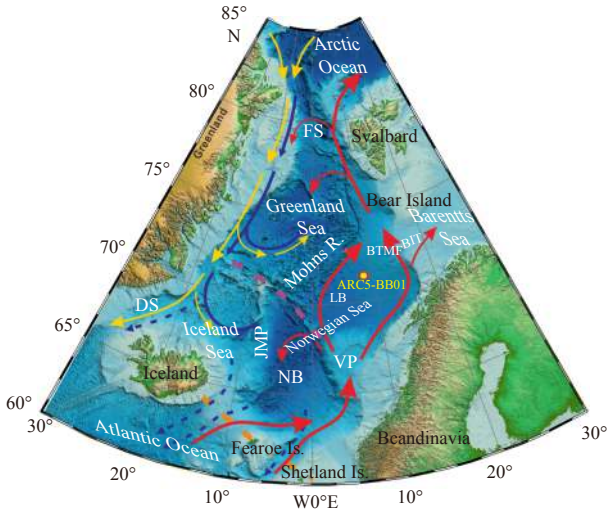

Fig. 1. Oceanography setting and location of core ARC5-BB01. Red solid arrow indicates Norwegian Atlantic Current; yellow and blue solid arrows indicate surface and bottom East Greenland Current, respectively; blue dashed arrow indicates Nordic overflow; purple dashed line indicates Jan Mayen Fracture Zone; orange dashed line indicates Iceland-Shetland Ridge; BIT, Bear Island Trough; BTMF, Bear Island Trough Mouth Fan; DS, Denmark Strait; FS, Fram Strait; JMR, Jan Mayen Ridge; LB, Lofoten Basin; NB, Norwegian Basin; VP, Vøring Plateau

Owing to the inflow of the warm NAC, no sea ice forms in the Norwegian Sea nowadays. In contrast, during the last glaciation, the warm NAC weakened and sank beneath the low-temperature, low-salinity polar water layer to form an intermediate water layer (Ezat et al., 2014), resulting in weakened convection and ventilation in the Norwegian Sea. The expansion and retreat of sea ice varied consistently with rapid climate change (Sarnthein et al., 2003; Hoff et al., 2016). In the last glacial maximum (LGM), the BIS on the eastern side of the Norwegian Sea extends up to the shelf edge (Spielhagen et al., 2004; Patton et al., 2017). An approximately 100-km-long trough known as the Bear Island Trough was eroded on the Barents Shelf south of Bear Island as the glacier was moving toward the Norwegian Sea, and fan-shaped, glacial debris-flow deposits formed at the end of the BIT (Fig. 1). These deposits are now known as the Bear Island Trough Mouth Fan (BTMF). The lobe of the glacial debris fan extended southwestward from the upper continental slope to locations with a water depth of 2 600 m, covering a total area of 28×10^4 km^2 (Andreassen et al., 2008).

3 Materials and methods

The sediment core ARC5-BB01 (hereafter BB01) used in this study was collected using a gravity core sampler aboard icebreaker R/V *Xuelong* in the northern Norwegian Sea (71°45.81′N, 8°56.94′E, 2 613 m water depth) at the edge of the BTMF (Fig. 1) during the 5th Chinese Arctic Research Expedition (CHINARE) in 2012. The core is 4.25 m in length.

The top 10 cm of the core was sampled at 2-cm intervals, and the rest at 1-cm intervals. Before sampling, the color of the sediment was measured using a CM700D spectrophotometer to obtain the Hunter color values L* (lightness), a* (redness-greenness), and b* (yellowness-blueness), which were then converted to RGB color values and plotted as a color profile.

For grain size analysis, the samples were preprocessed in the

following steps: (1) about 0.7 g sediment sample was placed into a beaker, to which was added 10–30 mL of 30% hydrogen peroxide (H_2O_2) and kept for 24 h in order to remove organic matter; (2) 30 mL of 10% hydrochloric acid (HCl) was added, and the mixture was settled at room temperature (20–25°C) for 24 h in order to remove calcareous biological debris; (3) about 1 000 mL of deionized water was added and the sample mixture was kept 24 h to rinse acidic ions; (4) after removing the supernatant from the beaker with a glass pipette, 20 mL of 1 mol/L sodium carbonate (Na_2CO_3) was added to remove siliceous biological debris; (5) 10 mL of 0.5 N sodium hexametaphosphate ($[NaPO_3]_6$) was added to the beaker and the resulting mixture was subject to ultrasonic dispersion for 10 min before instrumental analysis; and (6) the sample was subject to grain size measurement on a MasterSizer 2000 laser grain analyzer at the Third Institute of Oceanography, Ministry of Natural Resources. The MasterSizer 2000 has a measurement range of 0.02–2 000 μm, and a grain-size resolution of 0.166φ in interval ($\varphi = -\log_2 D$, where D is the grain size in mm), thus yielding 100 grain-size fractions with a relative error of repeated measurements <3%.

The GSD fitting and partition were performed using the GrainAnalysis software. The software was developed by Xiaoguang Qin from the Institute of Geology and Geophysics, Chinese Academy of Sciences. The theory of the GSD partition is that the sediments with asymmetric or skewed grain size distributions are composed of two or more grain populations with symmetric log-normal distributions (Ashley, 1978; Qin et al., 2005) and the formula of the log-normal distribution function is expressed as follows:

$$F(x) = \sum_{i=1}^{n} \left[\frac{c_i}{\sigma_i \sqrt{2\pi}} \int_{-\infty}^{\infty} \exp\left(-\frac{(x-a_i)^2}{2\sigma_i^2} \right) \mathrm{d}x \right], \quad (1)$$

where n is the number of population and i is the ith grain population; $x = \ln(d)$, where d is the particle size (μm); c_i is the percentage of the ith grain population relative to the total sample, and a_i and σ_i are the average and standard deviation of the ith population in the sample. The method and the operational procedures of GrainAnalysis software were presented by Qin et al. (2005) and Xiao et al. (2012).

Smear slides of sediment grains with size at about 4 μm, 8 μm and 16 μm were made to examine mineral composition with petrographic microscope. The particles with different sizes were taken according to Stokes' Law.

Accelerator mass spectrometry (AMS) ^{14}C dating was performed on planktonic foraminifera *Neogloboquadrina pachyderma* (sin.) from nine samples at Beta Analytic Inc. (USA) (Table 1). The dating results were calibrated using Marine20 database and Calib 8.1 software, and the local carbon reservoir correction (ΔR) was 66±25 (Heaton et al., 2020).

In order to provide additional age constraints, magnetic susceptibility (MS) was measured at 2-cm intervals, and the MS variations were correlated to the Greenland ice-core (GISP2) oxygen isotope record. Samples for MS measurement were freeze-dried and then dispersed with an agate mortar. Portions of 7 g to 10 g of the dry samples were packed into 8-cm^3 non-magnetic plastic cubes and subjected to MS measurement at 976 Hz with an MFK1-FA Kappabridge susceptibility meter. The MS values were normalized to sample mass.

4 Results

4.1 *Chronological framework*

Table 1 presents the AMS ^{14}C dating results of core BB01 samples. The ^{14}C age at 400 cm is older than 45 000 a BP, which exceeds the limit of AMS ^{14}C dating. The other eight ^{14}C ages increased with depth without age inversion (Fig. 2a). Depth-age transformation was performed based on the linear interpolation of ^{14}C dating to establish a preliminary depth-age framework for core BB01 (Fig. 2b). The magnetic minerals in the Norwegian Sea sediments mainly come from the volcanic area of the Iceland-Shetland ridge to the south, and were transported by NAC (Kissel, 2005). During warm periods, MS increased due to the enhancement of NAC, and vice versa. The climate of the Greenland ice sheet is closely related to changes in NAC; therefore, MS in the Norwegian Sea sediments and the oxygen isotope records of the Greenland ice core changed simultaneously and used as a time scale (Rasmussen et al., 1996; Dowdeswell et al., 1999; Kissel et al., 1999; Elliot et al., 2001; Rasmussen and Thomsen, 2009). The MS in the upper 350 cm of the core is well correlated with the oxygen isotope record of the GISP2 ice core (Fig. 2b). Below 350 cm, the MS is out of phase with the GISP2 isotope record because of the lack of ^{14}C age control point. Therefore, constrained by the ^{14}C ages, the age model of core BB01 was tuned to the time scale of the GISP2 ice core (Figs 2c and d). The results show that the bottom of core BB01 is approximately 62 ka BP; thus, core BB01 covers the marine isotope stage (MIS) 1–3.

4.2 *Sediment grain size distribution*

The sediments of core BB01 were mainly composed of silt and clay. The silt content was between 6.9% and 81.1%, with a mean of 57.7%, and the clay content was between 16.6% and 93.1%, with a mean size of 41.4% (Figs 3a and b). According to the changes in silt and clay content, the entire core is subdivided into three units with divisions at ages of 13 ka BP and 31 ka BP. In

Table 1. AMS ^{14}C dating results and calibrated dates for core BB01

Laboratory code	Depth/cm	δ^{13}C/‰	^{14}C age/a BP*	ΔR corrected ^{14}C age/a BP**	1σ calibrated age/cal a BP***
Beta-360794	1	+0.5	920±30	850±30	410–260
Beta-360795	50	+0.9	8 860±40	8 790±40	9 400–9 210
Beta-360796	100	–2.4	12 630±50	12 560±50	14 080–13 860
Beta-360797	150	–0.2	17 500±70	17 430±70	20 300–20 020
Beta-360798	200	–0.4	21 430±90	21 360±90	24 870–24 520
Beta-363798	250	0.0	28 490±160	28 420±160	31 800–31 390
Beta-363799	300	+0.2	35 230±300	35 160±300	39 650–39 110
Beta-363800	350	–0.9	41 930±630	41 860±630	44 390–43 350
Beta-363801	400	+0.9	>43 500		

Note: * the sample age after correction of isotopic fractionation; ** the sample age after subtracting the local reservoir (ΔR=66±25); *** the calendar age after calibration with Marine20 database.

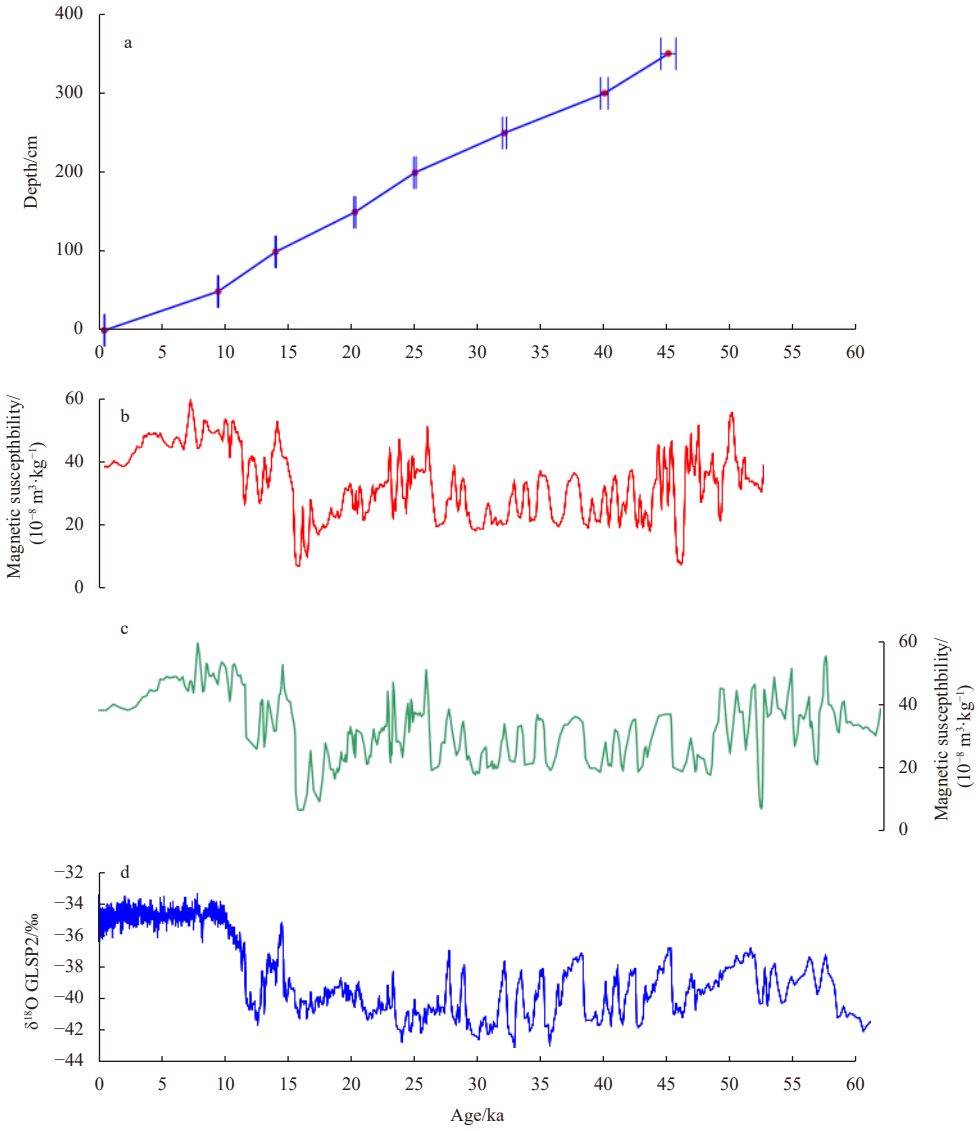

Fig. 2. Age-depth model for core BB01. a. Calibrated ^{14}C age versus depth. b. Magnetic susceptibility of core BB01 versus ^{14}C time scale. c. Magnetic susceptibility of core BB01 on GISP2 time scale. d. Oxygen isotope of GISP2 ice core versus age (Grootes et al., 1993).

the unit aged 31–13 ka BP, the silt content was significantly lower than that in the upper and lower units, while the clay content was generally higher. Moreover, the fluctuation amplitudes of silt and clay content in this unit were greater than those in the other two units. The sand content was relatively low (with a maximum content of 11.9%), including its absence in some layers. The sand content rapidly rises above 4% at layers unequally spaced by tens of centimeters, showing spikes in the content-age curve (Fig. 3c). The change in mean size was consistent with changes in silt and clay content (Fig. 3d). However, changes in the sorting coefficient, skewness, and kurtosis are not strongly consistent with changes in silt and clay content (Figs 3e–g).

4.3 *Characteristics of sediment grain size populations*

Figure 4 shows the representative GSDs of sediments in core BB01, which are all multimodal. A log-normal distribution function was used to decompose the GSDs of sediments in core BB01 into 3–4 populations; named from population 1 to population 4 (P1 to P4) in the order of increasing mode size.

The changes in the mode size and content of the populations in the sediments are shown in Fig. 5. The GSDs of sediments after 13 ka BP are composed of three populations, while the GSDs before 13 ka BP are composed of four populations. The mode size of P1 in sediments of the core was less than 1 μm, and the content of this population ranged from 2.9% to 24.8% (Figs 5a and b). The content of P1 at 31–13 ka BP was significantly higher than that in the upper and lower segments. The average content of P1 in this unit was 10.7%, while the mean contents of P1 after 13 ka and before 31 ka were 5.3% and 7.7%, respectively. Taking 13 ka as the boundary, the mode size and content of P2 and P3 are dramatically different in the upper and lower units. The mean mode size of P2 after 13 ka is 4.8 μm, and it decreased to 2.3 μm before 13 ka (Fig. 5c). The mean contents of P2 in these two units were 78.2% and 44.9%, respectively (Fig. 5d). For P3, the mean mode size in the two units are 16.6 μm and 6.8 μm (Fig. 5e), respectively, and the mean content are 16.6% and 39.5% (Fig. 5f), respectively. P4 was absent in the section after 13 ka. The mode size and content of P4 before 13 ka were 21.6 μm and 6.9% on average, respectively (Figs 5g and h).

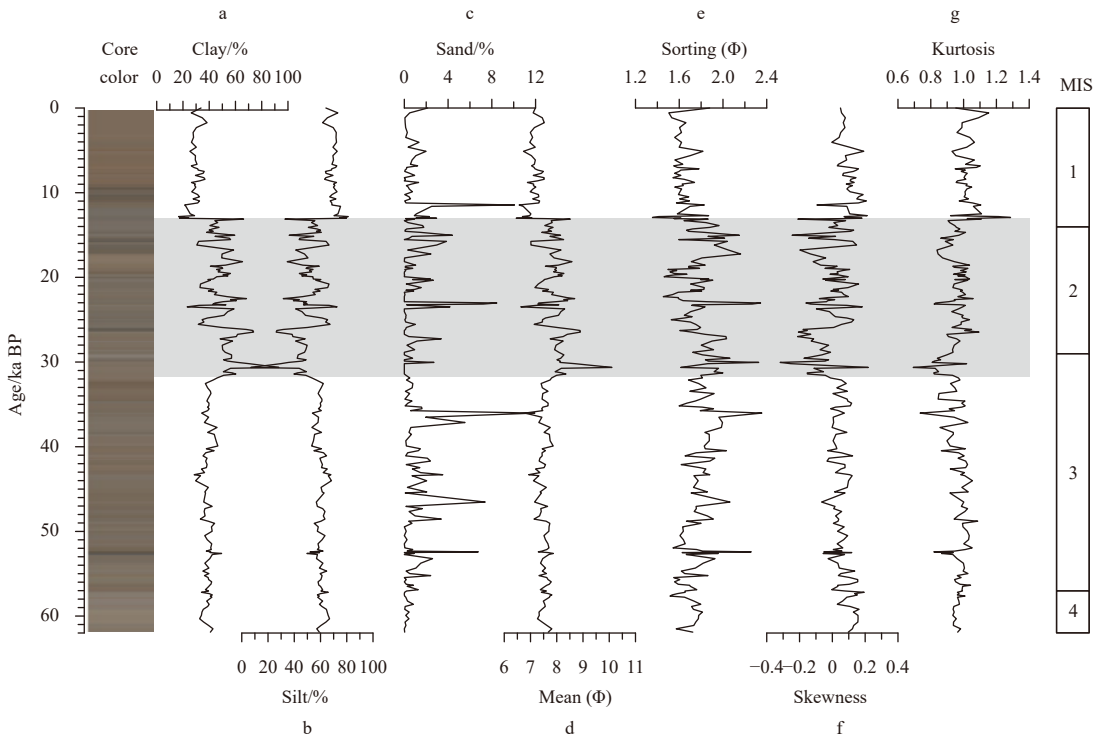

Fig. 3. The down core variations of clay, silt and sand content in sediments and their grain size parameters of core BB01.

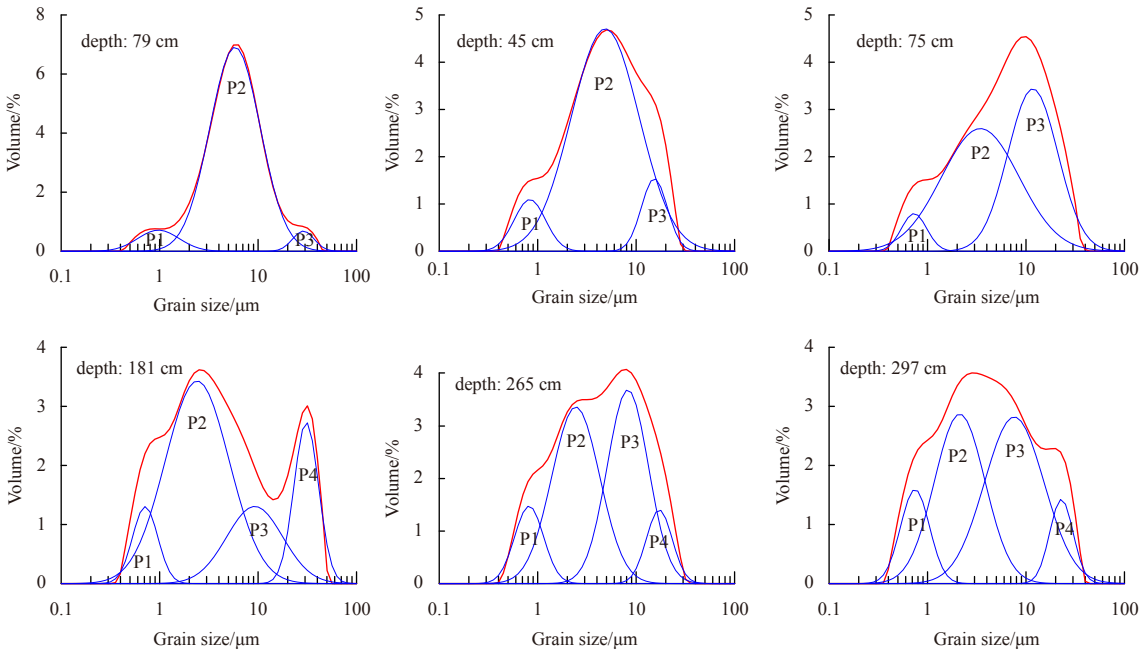

Fig. 4. Representative grain size distribution (red line) and their populations (blue line) of sediments in core BB01. P1, P2, P3, P4 are abbreviations of populations in grain size distribution in the order of mode size from fine to coarse.

5 Discussion

5.1 *Transportation mechanisms and origination of grains in different populations*

P4 is the coarsest population in sediments of core BB01, including grains (>154 μm) dominated by quartz, with grains of hematite-stained quartz and rock occurring sporadically (Fig. 6), which are derived from red bed deposits around the Nordic seas (Bond et al., 1997). The coarse grains in the high-latitude deep basin are referred to as IRD, which are transported by sea ice or icebergs. Sea ice is an important transport agent in high-latitude areas, especially in the Arctic Ocean. The Norwegian Sea is seasonally covered by sea ice during glacial periods (Sadatzki et al., 2019). However, sediments transported by sea ice are mostly fine-grained and contain little or no grains larger than 63 μm (Baumann et al., 1995). Frazil ice entrains fine suspended

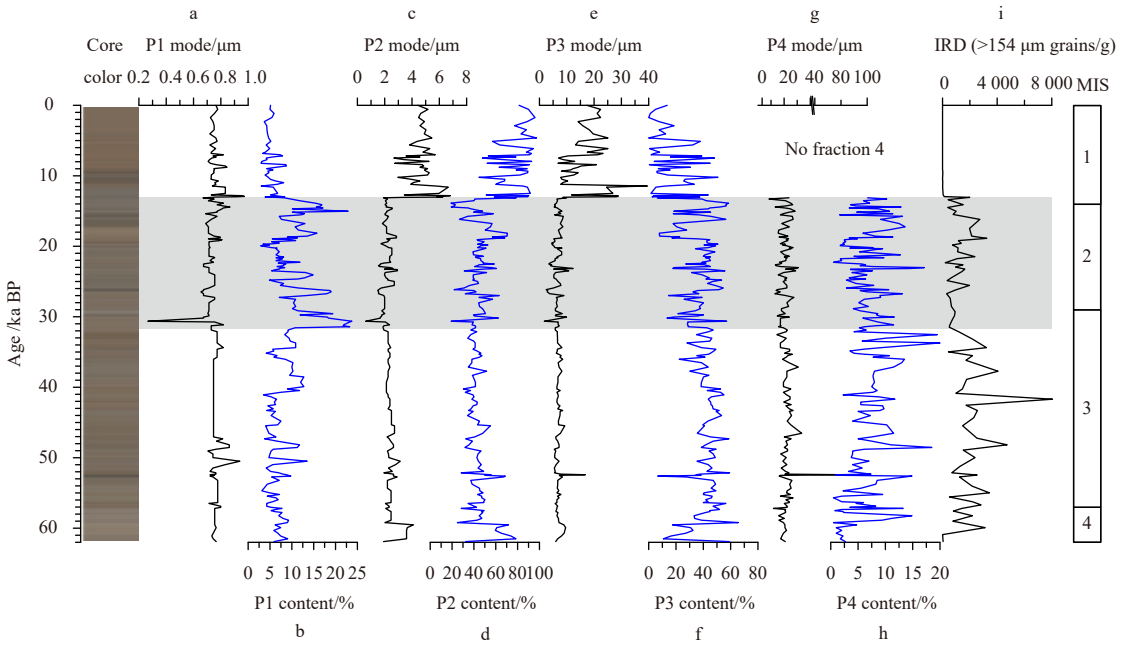

Fig. 5. Down core variation of mode size and content of each population in sediments of core BB01.

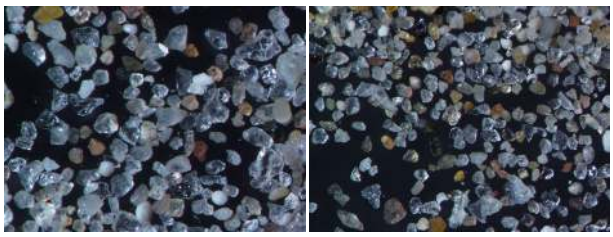

Fig. 6. IRD grains (>154 μm) in population 4 at 13 ka BP (left) and 33.4 ka BP (right) in core BB01.

particles in the water column with a mode size not larger than 10 μm (Darby et al., 2009), and the entrainment is most effective in water shallower than approximately 20 m (Eicken et al., 2005). Anchor ice occurs at depths of less than about 30–50 m and entrains whatever available sediments on the shallow sea floor with variable size (Darby et al., 2009). However, the potential role of anchor ice in sediment entrainment from the seafloor is assumed to be of lesser importance (Eicken et al., 2005). The northern Norwegian Sea is mainly composed of deep basins. There is no shallow continental shelf (<50 m) and super-cold conditions for anchor ice occurring during the last glaciation in the Norwegian Sea because the shallow shelf of the Norwegian Sea was covered by ice sheets during the last glaciation, as well as the Barents Shelf. Even if sea ice played a role in transporting P4, it was not the dominant transport agent. Alternatively, icebergs were more likely to be the dominant transport agents for P4.

It is worth noting that the mean mode size of P4 is far smaller than the grain size of conventional IRD (e.g., >63 μm, 125 μm, or 250 μm) (Spielhagen et al., 2004; Darby et al., 2006; Polyak et al., 2010). Icebergs can carry sediment grains of all sizes from clay to boulders (Polyak et al., 2010). However, conventional IRD analysis separates grains larger than a certain threshold from sediments and ignores fine grains and drop-stones transported by icebergs. According to the theory of sediment grain size distribution, the size of sediment grains related to a specific transport agent follows a log-normal distribution function (Ashley, 1978); thus, the conventional IRD only accounts for a small part of the particles in the icebergs. The northern Norwegian Sea is the dominant fate of melt water and icebergs from the BIS (Patton et al., 2017), and previous studies have demonstrated that the IRD in the northern Norwegian Sea originates from the BIS (Ruddiman, 1977; Lekens et al., 2006), along with the intermittent calving of the BIS and massive discharge of icebergs into the Norwegian Sea during the last glaciation (Dokken and Jansen, 1999), the grains of P4, including conventional IRD, were released by the melting of icebergs. In addition, both the content of P4 and conventional IRD in the core BB01 change with the same trend and disappear after 13 ka BP (Figs 5h and i), which corroborates that the P4 in the core BB01 is from BIS and icebergs are its transport agent, because the biomark IP_{25} demonstrated that the sea ice in the northern Norwegian Sea is abruptly terminated at 11.5 ka BP (Belt et al., 2015; Xiao et al., 2017), later than the age of P4 disappear. Therefore, icebergs rather than sea ice comprise the dominant transport agent of P4, and P4 is a proxy index of ice sheet evolution.

The sediments in core BB01 after 13 ka BP consisted of three populations. The mode size of the coarsest population after 13 ka BP is approximately 16 μm on average (Fig. 5e), which is slightly less than that of P4 before 13 ka BP (Fig. 5g). However, the composition of minerals in P3 after 13 ka BP is different from that in P4 before 13 ka BP, suggesting that the sources and transport agents of these two populations are different. Colorless flaky volcanic glass (opaque under cross-polarized light) is common in the coarsest population after 13 ka BP as well as in P2 and P3 before 13 ka BP (Figs 7a–f), whereas quartz (gray minerals under cross-polarized light) are dominant in P4 (Figs 7g and h), similar to the results of conventional IRD analysis (Fig. 6). The volcanic glass in the Norwegian Sea is derived from the Iceland-Shetland Ridge (Bond et al., 1997), an igneous province formed by the Iceland hotspot, and is transported by NAC to the Norwegian Sea. In comparison, the area underlying the BIS during the last glaciation is a stable Baltic Plate, sedimentary rocks including red beds occur and outcrop around the Barents Sea (Bond et al.,

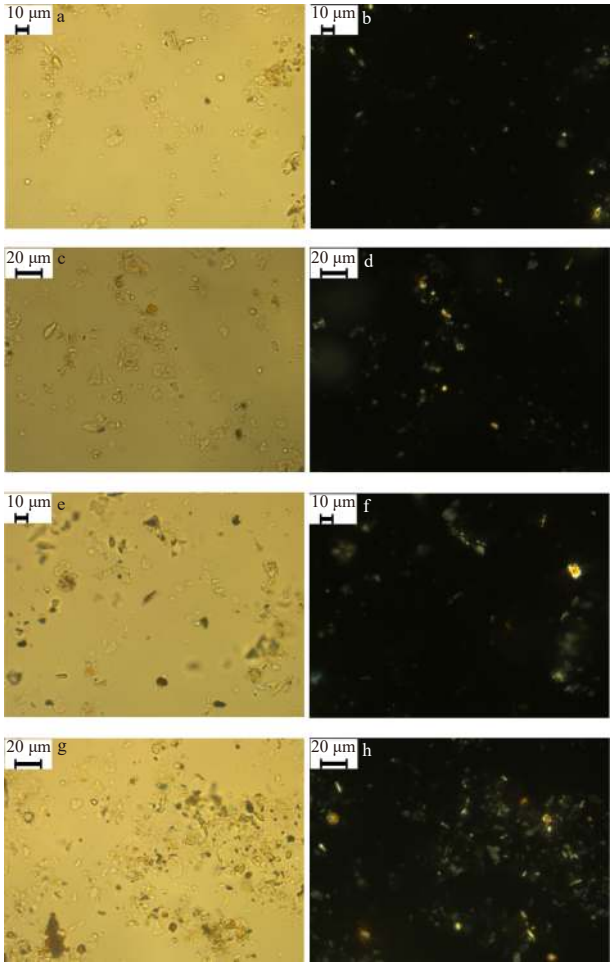

Fig. 7. Smear photomicrographs of sediment grains with different sizes in core BB01. Photos on the left panel are under plane-polarized light, and on the right panel are the same photos under cross-polarized light. a–d. Grains in P2 and P3 at 40 cm (after 13 ka BP); e and f. grains in P3 at 355 cm; g and h. grains in P4 at 355 cm, in which most of the grains are grey minerals (quartz) under cross-polarized light.

1997), and icebergs from BIS are the transport agents for P4. The negative correlation between the total content of P2 and P3 and the content of ice sheet related P4 suggests that P2 and P3 in sediments of core BB01 are not derived from the ice sheet (Fig. 8a). Therefore, the coarsest population after 13 ka BP belongs to P3 instead of P4, and the change in its mode size is the result of NAC evolution.

As mentioned above, volcanic glasses were present in both P2 and P3. The volcanic glasses are representative minerals from the volcanic area of the Iceland-Shetland Ridge to the south of the Norwegian Sea and transported northward by NAC into the Norwegian Sea (Bond et al., 1997). The value of magnetic susceptibility increased with the strengthening of the NAC during the interglacial and interstadial periods (Fig. 2). The positive correlation between the total content of P2 and P3 and the value of magnetic susceptibility (Fig. 9) also suggests that the changes in these two populations are related to the inflow of NAC into the Norwegian Sea.

There is a negative correlation between P2 and P3 contents and a positive correlation between P2 and P3 mode sizes in core BB01 (Figs 5c–f and 8b), which is difficult to explain by direct evidence. This may be the result of the NAC flowing into the Norwegian Sea with two branches (Fig. 1). The west branch flows between the Iceland and Faroe Islands, and the east branch flows through the channel between the Faroe and Shetland Islands. The latter is the main tributary of NAC, and the runoff is more than twice that of the former (Dickson and Brown, 1994; Rasmussen and Thomsen, 2008). However, the width of the submarine ridge between the Iceland and Faroe Islands, where the west branch flows through, is three times the width of the channel between the Faroe and Shetland Islands for the east branch. Therefore, the velocity of the NAC in the east branch is greater than that in the west branch owing to the smaller width of the water passages and the stronger NAC runoff passing through (Dickson and Brown, 1994). The different velocities of the two branches result in the two populations in sediments of core BB01 with different sizes (P2 and P3). Although the NAC was weakened and sank underneath the cold fresher melt water to become an intermediate water mass during the glacial period (Ezat et al., 2014), it still flowed into the Norwegian Sea in two branches and the east branch was still the main tributary (Rasmussen and Thomsen, 2008), which might have resulted in a decrease in P2 and P3 mode sizes before 13 ka BP. In addition, during the last glacial period, the weakened NAC sank to >1 200 m water depth (Dokken et al., 2013; Ezat et al., 2014) and contacted the bottom floor of the Iceland-Faroe submarine ridge but did not reach the bottom of the channel between the Faroe and Shetland Islands (Fig. 10a). Therefore, the area of the NAC winnowing sediments dominated by volcanic glass from the bottom of the west branch is larger than that in the east branch. Although the velocity and volume of the NAC in the west branch are lower than those in the east branch, owing to the larger area of the NAC connecting the seabed in the west branch, and the contents of P2 and P3 in the last glaciation are similar (Figs 5d and f). During the interglacial period, the enhancement of NAC in the two branches resulted in an increase in P2 and P3 mode sizes. The NAC in both branches moves upward and becomes a surface current (Fig. 10b). Because the water depth of the west branch is shallower than that of the east branch, the area of the NAC winnowing sediments from the bottom of the west branch is larger than that of the east branch. As a result, the content of P2 was higher than that of P3.

Although the sizes of P2 and P3 in core BB01 are similar to those of sediments entrained by frazil ice, P2 and P3 in core BB01 are less likely to be transported by frazil ice. Previous work has demonstrated that there is no sea ice in the North Atlantic Sea and Norwegian Sea during the interglacial and interstadial periods (Hoff et al., 2016); however, the content of P2 and P3 increased during the interglacial and interstadial periods (Fig. 11), suggesting that P2 and P3 are related to the NAC instead of sea ice.

P1 is the finest population in sediments of core BB01 and is composed of clayey grains, which can be transported by current for long distances and usually multi-source. The content of P1 increased significantly during 31–13 ka BP, a period spanning the last glacial maximum and deglaciation. Similar to the content of P1, the content of kaolinite in the clay fraction is strikingly higher during this period (data on clay minerals will be published separately and will not be discussed in detail here). The kaolinite in the northern Norwegian Sea is derived from the shelf of the Barents Sea (Kuhlemann et al., 1993), and the higher kaolinite content indicates that BIS is a contributor for P1 at 31–13 ka BP. Ice sheets (or icebergs) contain not only coarse sandy sediments (conventional IRD) but also clay or boulders (Clark and Hanson, 1983; Nürnberg et al., 1994; Baumann et al., 1995; Darby, 2003; Dethleff, 2005; Darby et al., 2009, 2011). The BIS to the east of the Nor-

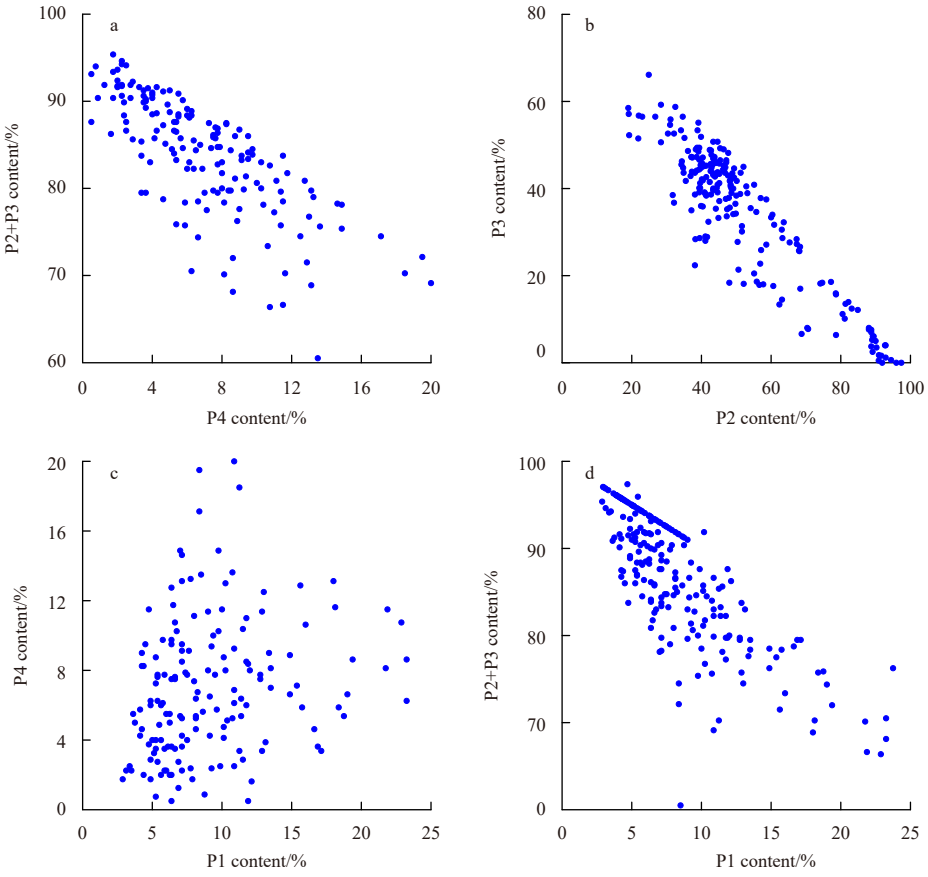

Fig. 8. Correlations between grain size populations in sediments of core BB01. P1–P4: population 1 to population 4.

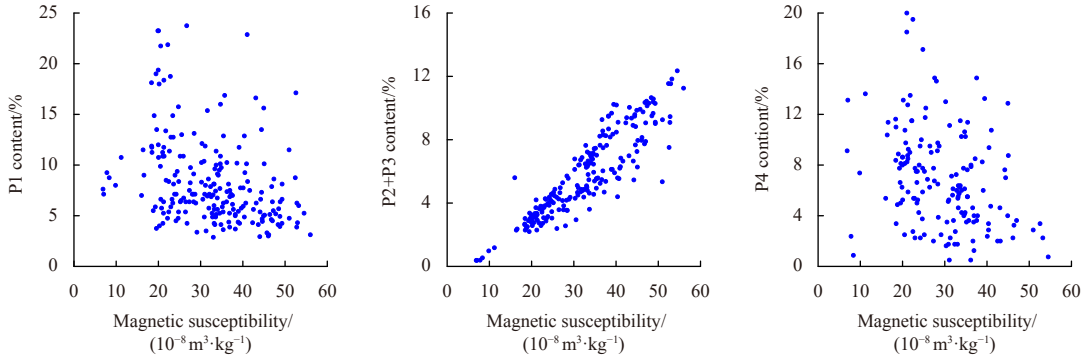

Fig. 9. Correlations between magnetic susceptibility and grain size population content in sediments of core BB01.

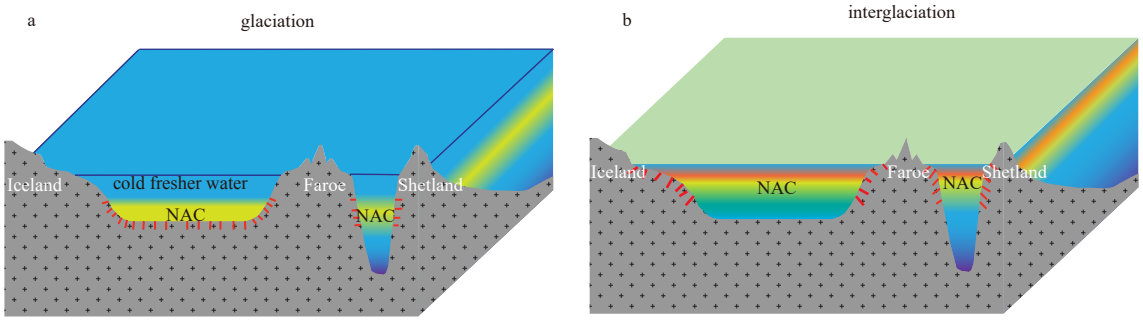

Fig. 10. Schematic showing North Atlantic Current (NAC) in water column during glacial (a) and interglacial periods (b).

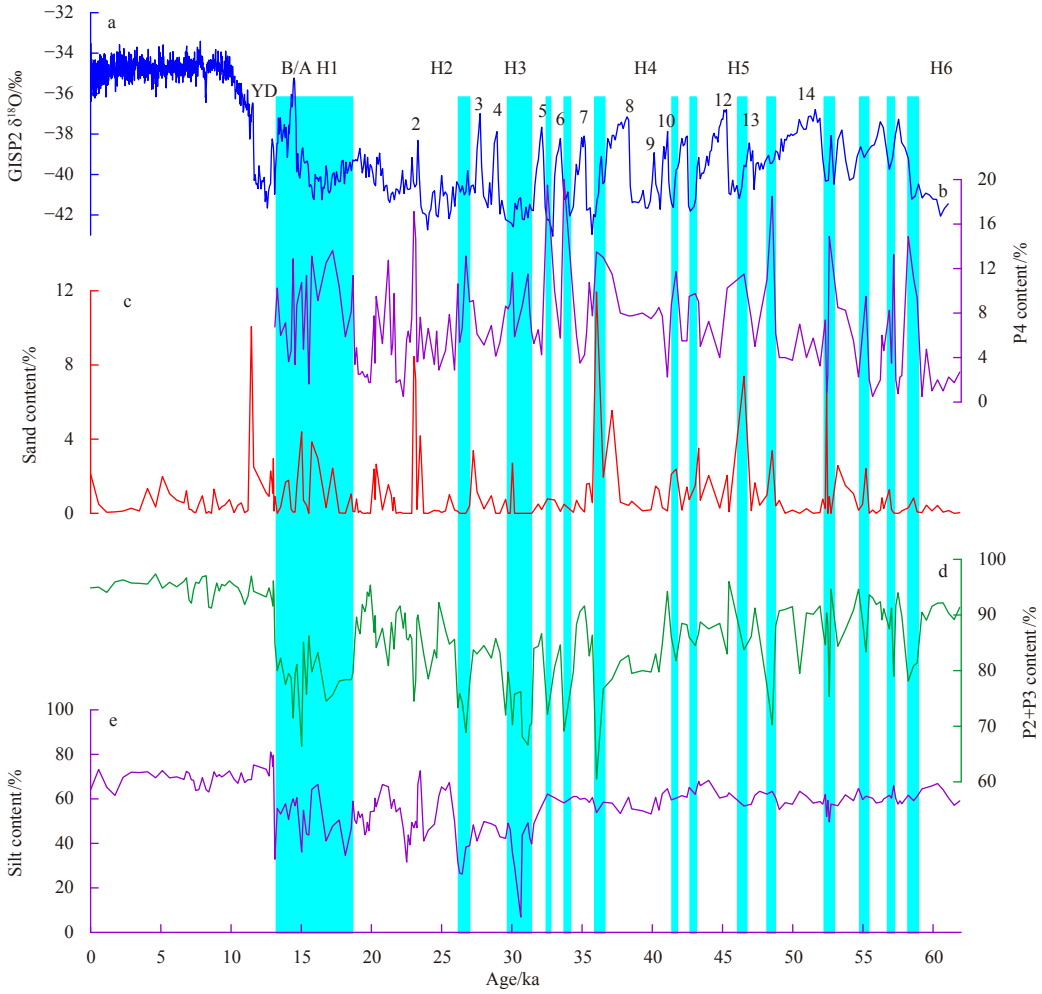

Fig. 11. Correlation of sand and silt content and P2+P3 and P4 content in sediments of BB01 core. Numbers over the GISP2 curve mark the position of the Dangaard-Oeschger interstadials; B/A- Bølling-Allerød warm period; H- Heinrich Event; YD- Younger Dryas.

wegian Sea advanced to a shelf break at approximately 30–29 ka BP (Baumann et al., 1995; Clark et al., 2009; Patton et al., 2017). A plume rich in clay occurs at the lead edge of the ice sheet (Wang and Hesse, 1996; Hesse et al., 1997). When the BIS advanced to a threshold location toward the Norwegian Sea direction, the plume could arrive at the site of core BB01, which increased the P1 content in the sediments. During the last deglacial period, along with the rapid ablation of the BIS, a massive flood of melt water was discharged into the northern Norwegian Sea. The clayey sediments in the BIS were released into the Norwegian Sea with the input of meltwater.

The contribution of NAC to P1 could not be ruled out. The marine environment of the Norwegian Sea was similar to modern conditions during the Holocene as a consequence of the warm NAC strengthening (Austin and Kroon, 2001). With the melting away of BIS after 13 ka BP (Hormes et al., 2013; Telesiński et al., 2015), the input of grains from the ice sheet was negligible. In addition, there was no river with a large amount of sediment input around the Norwegian Sea, and the contribution of the river to P1 was also ruled out. Turbidity deposits often cause Bouma sequences and stratigraphic age reversal. No turbidity deposits are found in core BB01, so the fine sediments formed by turbidity currents are not discussed here. Alternatively, P1 in the Holocene may have been derived from NAC. Because the sediment particles transported by NAC were mainly composed of silty grains (P2 and P3 in sediments), and without the contribution of BIS, the content of P1 in core BB01 was lower after 13 ka BP than before.

5.2 *Validity of grain size populations as proxies of paleoceanographic evolution*

The conventional IRD is a part, but not all, of the ice sheet-related P4 in sediments of core BB01. To further compare the iceberg and ice sheet evolution information represented by the content of >63 μm sand versus the content of P4 in the BB01 core, the two contents were compared with the oxygen isotope record of the GISP2 ice core (Fig. 11a). The peaks of the sands correspond to a high content of P4. In comparison, P4 provided more detailed information about the evolution of icebergs or ice sheets than that from conventional IRD (Figs 11b and c). The changes in the content of P4 are synchronous with the changes in the GISP2 oxygen isotope record, with the latter being an indicator of temperature changes. Especially in MIS 3, the peak abundances of P4 coincided with stadials. Increases in IRD content during stadials have also been observed in other regions of the Norwegian Sea (Rasmussen et al., 1996; Dokken and Jansen, 1999; Elliot et al., 2001). The strong correlation between P4 content and oxygen isotopes of the GISP2 ice core suggests that P4 can be used as an effective proxy for ice sheet evolution. The high content of P4 in stadials during MIS3 indicated the calving of the BIS and massive

discharge of icebergs.

The changes in P2 and P3 in sediments of core BB01 were related to the variation in NAC. The total content of P2 and P3 decreased at stadials during MIS3 (Fig. 11d), suggesting that the strength of NAC was weakened due to the increase in melt water, as indicated by the increase in P4 content. The variation in silty content in sediments of core BB01 during MIS3 was nearly constant and was insensitive to stadial and interstadial (Fig. 11e). Thus, P2 and P3 can also be used as an effective proxy for NAC in the northern Norwegian Sea.

5.3 *Evolution of NAC and BIS in the northern Norwegian Sea*

As described, the changes in the grain size populations of core BB01 were controlled by the evolution of ice sheets and ocean currents. In MIS 3–4 before 31 ka BP, the change in P4 in core BB01 was synchronous with the Greenland ice-core record. During each stadial, the sharp increase in P4 content indicates that the collapse of the BIS was accelerated, and a large volume of icebergs from the BIS entered the northern Norwegian Sea. In contrast, the icebergs discharged into the northern Norwegian Sea decreased during the interstadial period. The decreased mode sizes of P2 and P3 indicate that the NAC weakened before 31 ka BP (Fig. 5).

By 31 ka BP, the content of P1 in sediments of core BB01 increased abruptly, indicating that the BIS had advanced nearly to the edge of the shelf (Spielhagen et al., 2004; Patton et al., 2017), and the plumes rich in clayey sediments formed in the lead edge of the BIS and drifted into the northern Norwegian Sea. Consequently, the sediments in the northern Norwegian Sea are characterized by a high clay content. The P4 content fluctuated periodically at 31–19 ka BP, indicating intermittent calving of BIS during the LGM, similar to that in MIS3. The BIS began to shrink after 19 ka BP (Lekens et al., 2005; Eldevik et al., 2014; Telesiński et al., 2015). With the rapid ablation of the BIS, massive flooding of melt water containing clayey sediments and icebergs discharged into the northern Norwegian Sea through the Bear Island Trough on the Barents Shelf (Andreassen et al., 2008; Patton et al., 2017), and the northern Norwegian Sea has long received the inputs of clayey grains (P1) and coarse grains (P4) from ice sheet ablation until the BIS was ablated completely at 13 ka BP (Telesiński et al., 2015; Patton et al., 2017; Xiao et al., 2017).

The strength of NAC at 31–13 ka BP was still weak, as indicated by the lower mode sizes of P2 and P3. This unique depositional environment continued until the end of the Bølling-Allerød warm period in the late deglaciation (13 ka BP), when the BIS was ablated completely (Telesiński et al., 2015; Patton et al., 2017; Xiao et al., 2017). The P4 in sediments of core BB01 disappeared after 13 ka BP, and the content of P1 decreased significantly. Without the impact of melt water from the BIS, the NAC flowing into the Norwegian Sea strengthened abruptly, as indicated by the abrupt increase in the mode sizes of P2 and P3. The oceanographic environment in the northern Norwegian Sea transformed from the control of BIS to the control of NAC, similar to the present state. The abrupt enhancement of NAC subsequent to the melting away of BIS suggests that the BIS controls the strength of the NAC inflow into the Norwegian Sea.

6 Conclusions

The sediments of core BB01 sampled from the northern Norwegian Sea are mainly composed of clay and silt with a small proportion of sandy grains, which were decomposed into 3–4 grain size populations with a log-normal distribution function. Among them, clayey population 1 was derived from the NAC and BIS plumes, silty populations 2 and 3 were derived from the NAC flowing into the Norwegian Sea, and population 4 was derived from the melting of icebergs and BIS ablation.

Based on changes in the content and size of each population, core BB01 was subdivided into three units with divisions at 13 ka BP and 31 ka BP, representing three stages of paleoceanographic evolution in the northern Norwegian Sea since 60 ka BP. In particular, at 60–31 ka BP, the content of population 4 increased in stadials, indicating that the icebergs discharging into the northern Norwegian Sea increased in stadials. At 31–13 ka BP, the content of population 1 was significantly higher due to the plume formed in the lead edge of the BIS, and the northern Norwegian Sea was under the strong influence of melt water, while the NAC was still relatively weak, as indicated by the mode size of populations 2 and 3. The content of population 4 fluctuated during the LGM, indicating intermittent calving of the BIS and discharge of icebergs. From 19–13 ka BP, the constant high content of P1 and P4 in sediments demonstrates the ongoing ablation of BIS. After 13 ka BP, the NAC suddenly became stronger, as indicated by the increased mode size of populations 2 and 3, and the sediment layers no longer contained ice sheet-related population 4, indicating that the northern Norwegian Sea was no longer affected by melted ice water and changed back into a marine environment controlled by the warm Atlantic Current.

Acknowledgements

We are grateful to Jule Xiao and Xiaoguang Qin for providing grain-size analysis software and guidance, and two anonymous reviewers for their valuable suggestions which have improved the manuscript. We also thank all the crew members of the 5th Chinese Arctic Research Expedition (CHINARE) and all the scientific research team members in charge of geological sampling.

References

Aksenov Y, Bacon S, Coward A C, et al. 2010. The North Atlantic inflow to the Arctic Ocean: High-resolution model study. Journal of Marine Systems, 79(1–2): 1–22, doi: 10.1016/j.jmarsys.2009.05.003

Andreassen K, Laberg J S, Vorren T O. 2008. Seafloor geomorphology of the SW Barents Sea and its glaci-dynamic implications. Geomorphology, 97(1–2): 157–177, doi: 10.1016/j.geomorph.2007.02.050

Ashley G M. 1978. Interpretation of polymodal sediments. The Journal of Geology, 86(4): 411–421, doi: 10.1086/649710

Austin W E N, Kroon D. 2001. Deep sea ventilation of the northeastern Atlantic during the last 15, 000 years. Global and Planetary Change, 30(1–2): 13–31, doi: 10.1016/S0921-8181(01)00074-1

Bauch H A, Erlenkeuser H, Spielhagen R F, et al. 2001. A multiproxy reconstruction of the evolution of deep and surface waters in the subarctic Nordic seas over the last 30, 000 yr. Quaternary Science Reviews, 20(4): 659–678, doi: 10.1016/S0277-3791(00)00098-6

Baumann K H, Lackschewitz K S, Mangerud J, et al. 1995. Reflection of scandinavian ice sheet fluctuations in norwegian sea sediments during the past 150, 000 years. Quaternary Research, 43(2): 185–197, doi: 10.1006/qres.1995.1019

Belt S T, Cabedo-Sanz P, Smik L, et al. 2015. Identification of paleo Arctic winter sea ice limits and the marginal ice zone: Optimised biomarker-based reconstructions of late Quaternary Arctic sea ice. Earth and Planetary Science Letters, 431: 127–139, doi: 10.1016/j.epsl.2015.09.020

Bond G, Showers W, Cheseby M, et al. 1997. A pervasive millennial-scale cycle in North Atlantic Holocene and glacial climates. Science, 278(5341): 1257–1266, doi: 10.1126/science.278.5341.1257

Broecker W S. 1991. The great ocean conveyor. Oceanography, 4(2): 79–89, doi: 10.5670/oceanog.1991.07

Clark P U, Dyke A S, Shakun J D, et al. 2009. The last glacial maximum. Science, 325(5941): 710–714, doi: 10.1126/science.1172873

Clark D L, Hanson A. 1983. Central Arctic Ocean sediment texture: a key to ice transport mechanisms. In: Molnia B F, ed. Glacial-Marine Sedimentation. Boston, MA,USA: Springer, 301–330, doi: 10.1007/978-1-4613-3793-5_7

Darby D A. 2003. Sources of sediment found in sea ice from the western Arctic Ocean, new insights into processes of entrainment and drift patterns. Journal of Geophysical Research: Oceans, 108(C8): 3257, doi: 10.1029/2002JC001350

Darby D A, Myers W B, Jakobsson M, et al. 2011. Modern dirty sea ice characteristics and sources: The role of anchor ice. Journal of Geophysical Research: Oceans, 116: C09008, doi: 10.1029/2010JC006675

Darby D A, Ortiz J, Polyak L, et al. 2009. The role of currents and sea ice in both slowly deposited central Arctic and rapidly deposited Chukchi–Alaskan margin sediments. Global and Planetary Change, 68(1–2): 58–72, doi: 10.1016/j.gloplacha.2009.02.007

Darby D A, Polyak L, Bauch H A. 2006. Past glacial and interglacial conditions in the Arctic Ocean and marginal seas–a review. Progress in Oceanography, 71(2–4): 129–144, doi: 10.1016/j.pocean.2006.09.009

Dethleff D. 2005. Entrainment and export of Laptev Sea ice sediments, Siberian Arctic. Journal of Geophysical Research: Oceans, 110(C7): C07009, doi: 10.1029/2004JC002740

Dickson R R, Brown J. 1994. The production of North Atlantic Deep Water: Sources, rates, and pathways. Journal of Geophysical Research: Oceans, 99(C6): 12319–12341, doi: 10.1029/94JC00530

Dokken T M, Jansen E. 1999. Rapid changes in the mechanism of ocean convection during the last glacial period. Nature, 401(6752): 458–461, doi: 10.1038/46753

Dokken T M, Nisancioglu K H, Li C, et al. 2013. Dansgaard-Oeschger cycles: Interactions between ocean and sea ice intrinsic to the Nordic seas. Paleoceanography, 28(3): 491–502, doi: 10.1002/palo.20042

Dowdeswell J A, Elverhøi A, Andrews J T, et al. 1999. Asynchronous deposition of ice-rafted layers in the Nordic seas and North Atlantic Ocean. Nature, 400(6742): 348–351, doi: 10.1038/22510

Eicken H, Gradinger R, Gaylord A, et al. 2005. Sediment transport by sea ice in the Chukchi and Beaufort Seas: Increasing importance due to changing ice conditions?. Deep-Sea Research Part II: Topical Studies in Oceanography, 52(24–26): 3281–3302, doi: 10.1016/j.dsr2.2005.10.006

Eldevik T, Risebrobakken B, Bjune A E, et al. 2014. A brief history of climate–the northern seas from the Last Glacial Maximum to global warming. Quaternary Science Reviews, 106: 225–246, doi: 10.1016/j.quascirev.2014.06.028

Elliot M, Labeyrie L, Dokken T, et al. 2001. Coherent patterns of ice-rafted debris deposits in the Nordic regions during the last glacial (10–60 ka). Earth and Planetary Science Letters, 194(1–2): 151–163, doi: 10.1016/S0012-821X(01)00561-1

Ezat M M, Rasmussen T L, Groeneveld J. 2014. Persistent intermediate water warming during cold stadials in the southeastern Nordic seas during the past 65 k.y. Geology, 42(8): 663–666, doi: 10.1130/G35579.1

Ezat M M, Rasmussen T L, Thornalley D J R, et al. 2017. Ventilation history of Nordic Seas overflows during the last (de)glacial period revealed by species-specific benthic foraminiferal ^{14}C dates. Paleoceanography, 32(2): 172–181, doi: 10.1002/2016PA003053

Grootes P M, Stuiver M, White J W C, et al. 1993. Comparison of oxygen isotope records from the GISP2 and GRIP Greenland ice cores. Nature, 366(6455): 552–554, doi: 10.1038/366552a0

Hansen B, Østerhus S. 2000. North Atlantic–Nordic Seas exchanges. Progress in Oceanography, 45(2): 109–208, doi: 10.1016/S0079-6611(99)00052-X

Heaton T J, Köhler P, Butzin M, et al. 2020. Marine20—The Marine Radiocarbon Age Calibration Curve (0–55, 000 cal BP). Radiocarbon, 62(4): 779–820, doi: 10.1017/RDC.2020.68

Hesse R, Khodabakhsh S, Klaucke I, et al. 1997. Asymmetrical turbid surface-plume deposition near ice-outlets of the Pleistocene Laurentide ice sheet in the Labrador Sea. Geo-Marine Letters, 17(3): 179–187, doi: 10.1007/s003670050024

Hoff U, Rasmussen T L, Stein R, et al. 2016. Sea ice and millennial-scale climate variability in the Nordic seas 90 kyr ago to present. Nature Communications, 7(1): 12247, doi: 10.1038/ncomms12247

Hormes A, Gjermundsen E F, Rasmussen T L. 2013. From mountain top to the deep sea–Deglaciation in 4D of the northwestern Barents Sea ice sheet. Quaternary Science Reviews, 75: 78–99, doi: 10.1016/j.quascirev.2013.04.009

Kissel C. 2005. Magnetic signature of rapid climatic variations in glacial North Atlantic, a review. Comptes Rendus Geoscience, 337(10–11): 908–918, doi: 10.1016/j.crte.2005.04.009

Kissel C, Laj C, Labeyrie L, et al. 1999. Rapid climatic variations during marine isotopic stage 3: magnetic analysis of sediments from Nordic Seas and North Atlantic. Earth and Planetary Science Letters, 171(3): 489–502, doi: 10.1016/S0012-821X(99)00162-4

Knies J, Köseoğlu D, Rise L, et al. 2018. Nordic Seas polynyas and their role in preconditioning marine productivity during the Last Glacial Maximum. Nature Communications, 9(1): 3959, doi: 10.1038/s41467-018-06252-8

Kuhlemann J, Lange H, Paetsch H. 1993. Implications of a connection between clay mineral variations and coarse grained debris and lithology in the central Norwegian-Greenland Sea. Marine Geology, 114(1–2): 1–11, doi: 10.1016/0025-3227(93)90036-U

Latarius K, Quadfasel D. 2016. Water mass transformation in the deep basins of the Nordic Seas: Analyses of heat and freshwater budgets. Deep-Sea Research Part I: Oceanographic Research Papers, 114: 23–42, doi: 10.1016/j.dsr.2016.04.012

Lekens W A H, Sejrup H P, Haflidason H, et al. 2005. Laminated sediments preceding Heinrich event 1 in the Northern North Sea and Southern Norwegian Sea: Origin, processes and regional linkage. Marine Geology, 216(1–2): 27–50, doi: 10.1016/j.margeo.2004.12.007

Lekens W A H, Sejrup H P, Haflidason H, et al. 2006. Meltwater and ice rafting in the southern Norwegian Sea between 20 and 40 calendar kyr B.P.: Implications for Fennoscandian Heinrich events. Paleoceanography, 21(3): PA3013, doi: 10.1029/2005PA001228

Lisitzin A P. 2010. Marine ice-rafting as a new type of sedimentogenesis in the Arctic and novel approaches to studying sedimentary processes. Russian Geology and Geophysics, 51(1): 12–47, doi: 10.1016/j.rgg.2009.12.002

Meland M Y, Dokken T M, Jansen E, et al. 2008. Water mass properties and exchange between the Nordic seas and the northern North Atlantic during the period 23–6 ka: Benthic oxygen isotopic evidence. Paleoceanography, 23(1): PA1210, doi: 10.1029/2007PA001416

Middleton G V. 1976. Hydraulic interpretation of sand size distributions. The Journal of Geology, 84(4): 405–426, doi: 10.1086/628208

Muschitiello F, D'Andrea W J, Schmittner A, et al. 2019. Deep-water circulation changes lead North Atlantic climate during deglaciation. Nature Communications, 10(1): 1272, doi: 10.1038/s41467-019-09237-3

Nagashima K, Asahara Y, Takeuchi F, et al. 2012. Contribution of detrital materials from the Yukon River to the continental shelf sediments of the Bering Sea based on the electron spin resonance signal intensity and crystallinity of quartz. Deep-Sea Research Part II: Topical Studies in Oceanography, 61-64: 145–154, doi: 10.1016/j.dsr2.2011.12.001

Nürnberg D, Wollenburg I, Dethleff D, et al. 1994. Sediments in Arctic sea ice: Implications for entrainment, transport and release. Marine Geology, 119(3–4): 185–214, doi: 10.1016/0025-3227(94)90181-3

Park C S, Hwang S, Yoon S O, et al. 2014. Grain size partitioning in loess–paleosol sequence on the west coast of South Korea using the Weibull function. CATENA, 121: 307–320, doi: 10.1016/j.catena.2014.05.018

Patton H, Hubbard A, Andreassen K, et al. 2017. Deglaciation of the

Eurasian ice sheet complex. Quaternary Science Reviews, 169: 148–172, doi: 10.1016/j.quascirev.2017.05.019

Phillips R L, Grantz A. 2001. Regional variations in provenance and abundance of ice-rafted clasts in Arctic Ocean sediments: implications for the configuration of late Quaternary oceanic and atmospheric circulation in the Arctic. Marine Geology, 172(1–2): 91–115, doi: 10.1016/S0025-3227(00)00101-8

Polyak L, Alley R B, Andrews J T, et al. 2010. History of sea ice in the Arctic. Quaternary Science Reviews, 29(15–16): 1757–1778, doi: 10.1016/j.quascirev.2010.02.010

Pope E L, Talling P J, Hunt J E, et al. 2016. Long-term record of Barents Sea Ice Sheet advance to the shelf edge from a 140, 000 year record. Quaternary Science Reviews, 150: 55–66, doi: 10.1016/j.quascirev.2016.08.014

Qin Xiaoguang, Cai Binggui, Liu T. 2005. Loess record of the aerodynamic environment in the east Asia monsoon area since 60, 000 years before present. Journal of Geophysical Research: Solid Earth, 110(B1): B01204, doi: 10.1029/2004JB003131

Rasmussen T L, Thomsen E. 2008. Warm Atlantic surface water inflow to the Nordic seas 34–10 calibrated ka B.P. Paleoceanography, 23: PA1201, doi: 10.1029/2007PA001453

Rasmussen T L, Thomsen E. 2009. Ventilation changes in intermediate water on millennial time scales in the SE Nordic seas, 65–14 kyr BP. Geophysical Research Letters, 36(1): L01601, doi: 10.1029/2008GL036563

Rasmussen T L, Thomsen E, Moros M. 2016. North Atlantic warming during Dansgaard-Oeschger events synchronous with Antarctic warming and out-of-phase with Greenland climate. Scientific Reports, 6: 20535, doi: 10.1038/srep20535

Rasmussen T L, Thomsen E, van Weering T C E, et al. 1996. Rapid changes in surface and deep water conditions at the Faeroe Margin during the last 58, 000 years. Paleoceanography, 11(6): 757–771, doi: 10.1029/96PA02618

Ruddiman W F. 1977. Late Quaternary deposition of ice-rafted sand in the subpolar North Atlantic (lat 40° to 65°N). Geological Society of America Bulletin, 88(12): 1813–1827, doi: 10.1130/0016-7606(1977)88<1813:LQDOIS>2.0.CO;2

Sadatzki H, Dokken T M, Berben S M P, et al. 2019. Sea ice variability in the southern Norwegian Sea during glacial Dansgaard-Oeschger climate cycles. Science Advances, 5(3): eaau6174, doi: 10.1126/sciadv.aau6174

Sarnthein M, Pflaumann U, Weinelt M. 2003. Past extent of sea ice in the northern North Atlantic inferred from foraminiferal paleotemperature estimates. Paleoceanography, 18(2): 1047, doi: 10.1029/2002PA000771

Simstich J, Lorenz S J, Bauch H A. 2013. Reprint of: Evaluation of past stratification changes in the Nordic Seas by comparing planktonic foraminiferal $\delta^{18}O$ with a solar-forced model. Marine Micropaleontology, 99: 45–50, doi: 10.1016/j.marmicro.2013.03.009

Spielhagen R F, Baumann K H, Erlenkeuser H, et al. 2004. Arctic Ocean deep-sea record of northern Eurasian ice sheet history. Quaternary Science Reviews, 23(11–13): 1455–1483, doi: 10.1016/j.quascirev.2003.12.015

Struve T, Roberts N L, Frank M, et al. 2019. Ice-sheet driven weathering input and water mass mixing in the Nordic Seas during the last 25, 000 years. Earth and Planetary Science Letters, 514: 108–118, doi: 10.1016/j.epsl.2019.02.030

Sun Donghuai, Bloemendal J, Rea D K, et al. 2002. Grain-size distribution function of polymodal sediments in hydraulic and aeolian environments, and numerical partitioning of the sedimentary components. Sedimentary Geology, 152(3–4): 263–277, doi: 10.1016/S0037-0738(02)00082-9

Telesiński M M, Bauch H A, Spielhagen R F, et al. 2015. Evolution of the central Nordic Seas over the last 20 thousand years. Quaternary Science Reviews, 121: 98–109, doi: 10.1016/j.quascirev.2015.05.013

Wang Dong, Hesse R. 1996. Continental slope sedimentation adjacent to an ice-margin. II. Glaciomarine depositional facies on labrador slope and glacial cycles. Marine Geology, 135(1–4): 65–96, doi: 10.1016/S0025-3227(96)00012-6

Wang Qiang, Wekerle C, Wang Xuezhu, et al. 2020a. Intensification of the Atlantic water supply to the Arctic Ocean through fram strait induced by Arctic sea ice decline. Geophysical Research Letters, 47(3): e2019GL086682, doi: 10.1029/2019GL086682

Wang Weiguo, Yang Jichao, Zhao Mengwei, et al. 2020b. Spatial variation in grain-size population of surface sediments from northern Bering Sea and western Arctic Ocean: implications for provenance and depositional mechanisms. Advances in Polar Science, 31(3): 192–204, doi: 10.13679/j.advps.2020.0015

Wary M, Eynaud F, Rossignol L, et al. 2016. Norwegian Sea warm pulses during Dansgaard-Oeschger stadials: Zooming in on these anomalies over the 35–41 ka cal BP interval and their impacts on proximal European ice-sheet dynamics. Quaternary Science Reviews, 151: 255–272, doi: 10.1016/j.quascirev.2016.09.011

Xiao Jule, Chang Zhigang, Fan Jiawei, et al. 2012. The link between grain-size components and depositional processes in a modern clastic lake. Sedimentology, 59(3): 1050–1062, doi: 10.1111/j.1365-3091.2011.01294.x

Xiao Xiaotong, Zhao Meixun, Knudsen K L, et al. 2017. Deglacial and Holocene sea–ice variability north of Iceland and response to ocean circulation changes. Earth and Planetary Science Letters, 472: 14–24, doi: 10.1016/j.epsl.2017.05.006